Materials and Design 65 (2015) 862–868

Contents lists available at ScienceDirect

Materials and Design

journal homepage: www.elsevier.com/locate/matdes

Technical Report

Microstructure and micro-texture evolution during large strain deformation of an aluminium–copper–lithium alloy AA 2195

Niraj Nayan [a,*], Nilesh P. Gurao [b], S.V.S. Narayana Murty [a], Abhay K. Jha [a], Bhanu Pant [a], S.C. Sharma [a], Koshy M. George [a]

[a] Materials and Mechanical Entity, Vikram Sarabhai Space Centre, Trivandrum 695 022, India
[b] Department of Materials Science and Engineering, Indian Institute of Technology, Kanpur 208 016, India

ARTICLE INFO

Article history:
Received 12 July 2014
Accepted 11 September 2014
Available online 20 September 2014

ABSTRACT

A single hit, hot isothermal plane strain compression (PSC) test was used to understand the microstructural evolution during large strain deformation of aluminium–copper–lithium alloy AA 2195. Hot isothermal PSC tests were conducted in the temperature range of 300–450 °C and at strain rates of 0.01 s^{-1} and 1 s^{-1} with 75% thickness reduction. The flow curves during PSC exhibited weak softening at higher temperatures and dipping of the flow curve at a strain rate of 1 s^{-1}. Electron backscattered diffraction analysis (EBSD) of the PSC tested samples revealed that dynamic recrystallisation occurs in specimens deformed at higher temperatures and lower strain rates. It is possible to control the grain size in AA 2195 through the optimization of temperature and strain rate during thermo-mechanical processing.
© 2014 Elsevier Ltd. All rights reserved.

1. Introduction

Aluminium–copper–lithium alloys are being extensively used for aerospace applications [1] in view of their high specific strength, high stiffness and fracture toughness combined with good weldability. Al–Cu–Li alloys with controlled amount of alloying elements and in proper temper condition achieves ultrahigh strength and good fracture toughness at RT as well as cryogenic temperatures. These alloys are candidate materials for both earth storable and cryogenic propellants tanks of satellite launch vehicles [2]. These materials have been successfully used in NASA space shuttle, Falcon-9 [3], Air bus 380 and Boeing 777.

Aluminium–copper–lithium alloys for aerospace applications are required in the form of thick plates (of about 50 mm thickness) for the fabrication of propellant tanks (made by isogrid machining through pocket milling), sheets for gores, forgings for propellant and manhole covers and extrusions propellant feed lines. These are processed through a variety of manufacturing processes. These alloys are usually characterized by an unrecrystallised microstructure with highly elongated grains in the direction of rolling. The strong pancake type microstructure in aluminium–lithium alloys have been extensively studied and reported [4–6]. Microstructure of the material is critical in determining not only the mechanical properties of the material, but has a strong bearing on the corrosion and stress corrosion characteristics of the material during service. Further, it has been reported [7,8] that materials with coarse grains affect weldability. Since large sized space structures are manufactured by welding, it is essential to understand the microstructure and grain size control in the material. Since Al–Cu–Li alloys can be tempered to very high strength levels and are intended for critical aerospace applications, microstructural control is essential to ensure quality of the products realized. This necessitates detailed study on the microstructural evolution as a function of processing parameters such as strain, strain rate and temperature. Since the Al–Cu–Li alloys are produced from the direct chill casting in the form of ingots/slabs, they are hot rolled down to the required shapes such as plates/sheets/rolled rings. This thermo-mechanical processing step introduces very large strains and the strain rates encountered are usually high to improve the productivity. Therefore, a systematic study of the effect of processing parameters on the microstructural evolution in Al–Cu–Li alloy subjected to large strain deformation is essential.

Usually, high temperature deformation studies and microstructure optimization are carried out on hot compression tested specimens in a laboratory. This involves hot isothermal compression testing of solid cylindrical specimens deformed to 50% of their original height to obtain the stress–strain behavior under the processing conditions. Beyond 50% deformation, barreling of the cylindrical specimen takes place and therefore, large strain deformation behavior cannot be studied through hot isothermal compression testing. Here the flow curve is limited to a true strain of 0.7. However, in actual industrial thermo-mechanical processing, the strains involved are much higher. Therefore, a large strain

* Corresponding author. Tel.: +91 471 256 3944; fax: +91 471 270 5048.
E-mail addresses: metnayan@gmail.com, niraj_nayan@vssc.gov.in (N. Nayan).

http://dx.doi.org/10.1016/j.matdes.2014.09.037
0261-3069/© 2014 Elsevier Ltd. All rights reserved.

deformation technique is required to simulate the actual processing conditions. For this purpose, a single hit, hot isothermal plane strain compression testing has been used in the present study.

Therefore, the purpose of the present study is twofold; firstly to study the large strain deformation behavior by conducting hot isothermal single hit plane strain compression testing on Al–Cu–Li alloy AA 2195 and study the stress–strain behavior under large strain conditions; and secondly to evaluate the microstructure and micro-texture evolution of the deformed specimens to understand the mechanism of deformation under plane strain conditions.

2. Experimental details

A large strain single pass, simple compression technique extensively used by one of the co-authors [9–11] is utilized in the present study for conducting the large strain deformation studies. In contrast to the other large strain deformation processes where large strains are imposed by multi-pass deformation processes, this technique is a single pass deformation process. Thus this technique eliminates the possibility of the sample undergoing complex microstructural changes during static holding/reheating between the processing steps or avoids the sample undergoing complex multi-axial deformation. In the anvil compression test used in the present study, the strain imposed gets concentrated at the center of the specimen and the strain varies in the range of 0–4 from the surface to the center of the specimen. This strain distribution facilitates the observation of microstructures deformed to various strain levels in a single specimen. The strain distribution across the specimen and the methodology of testing used in the present study were discussed elsewhere in detail [9–11].

Test samples with dimensions of 15 mm × 13 mm × 12 mm were fabricated from the hot forged plates of AA 2195 alloy. The chemical composition of the alloy was 4.2Cu–1.1Li–0.35Mg–0.35Ag–0.15Zr–0.15Fe–0.10Si and balance-aluminium. The plates were realized from forging of as-cast and homogenized billets cast in vacuum induction melting furnace under inert atmosphere. The detail of the casting technique has been discussed elsewhere in details [12–14]. The specimens were machined from the hot forged plates in such a way that the compression axis is perpendicular to the forging direction. The initial microstructure of the material used in the present study is shown in Fig. 1. The material has elongated grains in the direction of perpendicular to the direction of forging.

Using a thermo-mechanical simulator capable of controlling the specimen temperature, strain and strain rate, plane strain compression tests were performed. Fig. 2 shows the schematic of the plane strain compression test conditions employed in the present study. As shown in Fig. 2, the specimens were heated to the desired temperature in the range of 300–450 °C. Heating of the specimen was done at 5 K s^{-1} from ambient temperature to the specified temperature by direct resistance and then compressed in a single stroke after soaking at the desired temperature for 60 s. The compressive deformation was carried out in the time periods of 1.38 s and 138 s so as to impose apparent nominal strain rates of

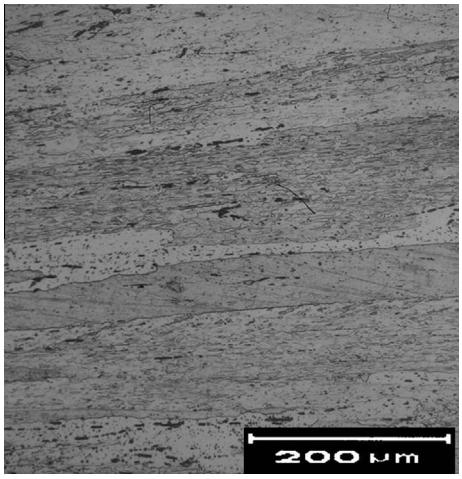

Fig. 1. Initial microstructure of the material used in the present study. The material is in as forged condition and has elongated grains in the direction of perpendicular to the direction of forging.

1 s^{-1} and 0.01 s^{-1}, respectively. Immediately after the deformation, the specimens were in-situ water quenched. Post compression, specimens were cut from the sample by a slow speed diamond saw for optical microscopy and EBSD analysis. Fig. 2(b) shows the schematic of the geometry of anvil compressed tested specimens and sectioning methodology adopted in the present study for microstructural observations.

Specimens for EBSD analysis after plane strain compression testing were carefully polished with mechanical polishing followed by electro polishing with Struers A2 solution containing perchloric acid, ethanol, butoxy ethanol and distilled water. The electron back scattered diffraction attached with FEI Quanta scanning electron microscope and TSL OIM 6 data collection and analysis software was used to collect and process the orientation information.

3. Results and discussion

3.1. Characteristics of flow curves

The microstructural evolution during hot deformation can be studied through the analysis of stress–strain curves [15–17]. Stress–strain curves are classified in to work-hardening type and dynamic recovery/dynamic recrystallisation type. The materials with strain hardening type curves are characterized by monotonic increase in flow stress with strain. The microstructures of these materials are characterized by deformed/compressed grains without any evidence of recovery/recrystallisation. On the other hand, the stress–strain curves exhibiting dynamic recovery/dynamic recrystallisation are characterized by flow softening immediately/after initial strain hardening. Fig. 3 shows the stress–strain curves of the samples deformed at different temperatures and strain rates. It can be noticed from Fig. 3 that as the temperature increases and $\dot{\varepsilon}$ decrease, the flow stress decreases. This flow softening after

Table 1
Variation of volume fraction of ⟨101⟩ fibre and different microstructural parameters determined from EBSD for differently processed AA 2195 samples.

Sample	Volume fraction of ⟨101⟩	Average misorientation (°)	Grain size (µm)	Grain orientation spread (GOS) (°)	Grain average misorientation (GAM) (°)
350 °C 10^{-2} s^{-1}	36.1	35.4	18.9	0.89	1.39
400 °C 10^{-2} s^{-1}	45.6	39.0	13.9	0.97	1.73
450 °C 10^{-2} s^{-1}	16.5	40.9	19.6	0.84	1.55
450 °C 10^{-1} s^{-1}	49.7	37.3	32	0.47	0.77

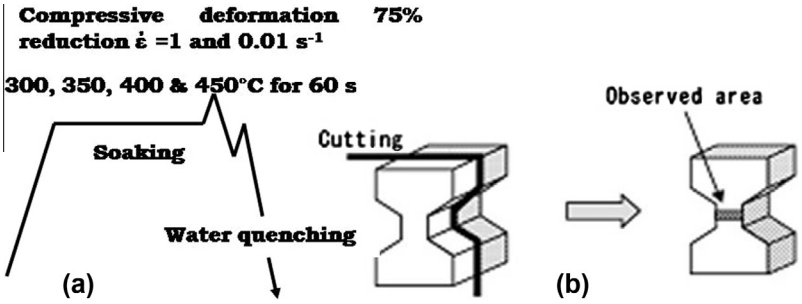

Fig. 2. Schematic of (a) the test conditions followed in the present study and (b) the anvil compressed specimen and sectioning methodology followed.

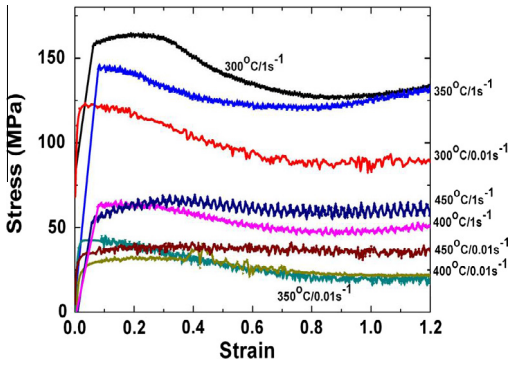

Fig. 3. Stress–strain curves of the plane strain compressed specimens deformed at different temperatures and strain rates.

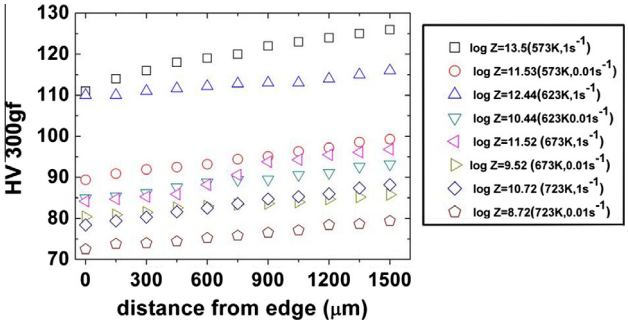

Fig. 4. Variation of vickers hardness with distance from the edge to the center of the plane strain compression tested samples tested at various temperatures and strain rates.

initial strain hardening is due to dominance of softening mechanism viz. dynamic recovery/recrystallization over strain hardening. The most noticeable fact is appearance of a trough in the flow curve at higher strain rate. This trough is also evident at low strain rates at 300 °C and 350 °C. Similar behavior was observed by Cheng et al in case of IN718 alloy [18]. Several reasons viz. strain induced phase transformation [19], softening due to texture [20], plastic instability and localization in shear bands [21], localized temperature rise due to adiabatic shear banding [22] have been suggested as the reason for flow softening. Here in case of Al–Li alloys, there is no phase transformation. Moreover, nature of deformation in plane strain compression is similar to that of rolling. Therefore, no textural change is expected during the test. Furthermore, adiabatic temperature rise would not happen due to high thermal conductivity and low strain rates applied in this study. So shear banding and recrystallization are the important contributors for the flow softening. It is important to note that shear banding and flow softening are interdependent. In other words, shear banding can cause flow softening; flow softening initiated by any other reasons can also cause shear banding.

In order to visualize the combined effect of strain rate and temperature on the flow behavior of material, Zener–Holloman (Z) parameter defined as $Z = \dot{\varepsilon}\exp(Q/RT)$ was used. In order to calculate Z, the value of Q for grain boundary diffusion has been used from Ref. [23]. Fig. 4 shows the variation of vickers hardness with distance from the edge of the plane strain compression tested samples to the center line of the deformed sample under various Z conditions. The distance from the edge to the center of the specimen is indicative of different stains from the edge ($\varepsilon = 0$) to the center line ($\varepsilon = 4.0$). It can be seen from Fig. 4 that at all temperatures and strain rates, work hardening type behavior is observed with a common general trend being stronger hardening with increasing Z parameter.

3.2. Effect of strain on microstructural evolution

Figs. 5 and 6 show the optical microstructures of specimens deformed different temperatures and strain rates used in the present study. In all cases microstructure has been taken from the center of the deformed sample for comparison purpose. At deformation temperature of 300 °C and 350 °C and strain rates of 1 $s^{-1}$and 0.01 s^{-1}, the microstructures are characterized by compressed grains without the evidence of any recrystallisation. On the other hand, the microstructures of specimens deformed at 400 °C and 450 °C at strain rates of 1 s^{-1} and 0.01 s^{-1}, the microstructures are characterized by the evidence of clear recrystallised grains. The presence of newly formed, strain free grains with wavy grain boundaries in specimens deformed at 400 °C and 450 °C is a clear indication of the occurrence of dynamic recrystallisation.

3.3. EBSD analysis

Fig. 7 shows the Inverse Pole Figure (IPF) map and image quality maps for the specimens deformed at various test conditions (350 °C at 10^{-2} s^{-1}; 400 °C at 10^{-2} s^{-1}; 450 °C at 10^{-2} s^{-1}; and 450 °C at 10^{-2} s^{-1}. These maps show elongated grains for all the samples. However, the image quality map shows the presence of sub-grains within the elongated grains. It is found that there is an increase in the formation of sub grains with increase in temperature at a fixed strain rate of 10^{-2} s^{-1}. It is also observed that there is a decrease in the extent of recrystallization at higher strain rate of 1 s^{-1} compared to 10^{-2} s^{-1} at 450 °C. Wavy boundaries clearly indicate the presence of dynamic recrystallization in the deformed microstructure at 450 °C sample tested at a strain rate of 10^{-2} s^{-1}. A closer look at the maps clearly shows that non ⟨101⟩ orientations undergo dynamic recrystallization with mostly ⟨100⟩ oriented grains showing grain fragmentation. A quantitative estimate of volume fraction of ⟨101⟩ fibre texture component and other microstructural parameters is given in Table 1 Misorientation

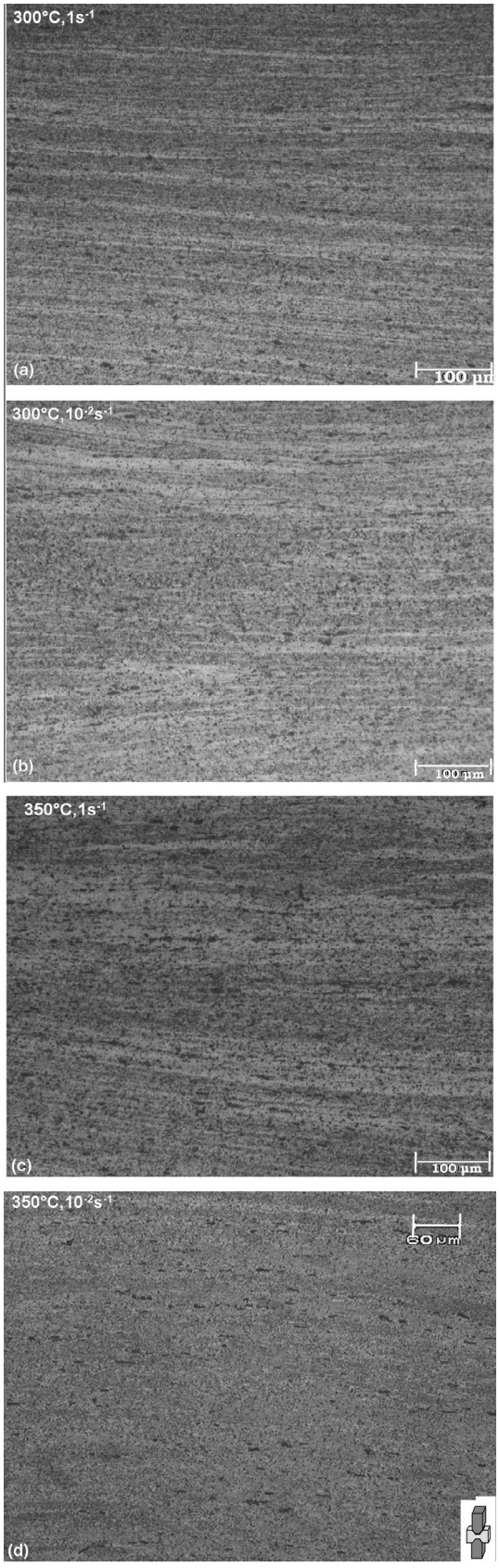

Fig. 5. Optical microstructures at the center of specimens deformed at (a): 300 °C and 1 s^{-1}; (b): 300 °C and 0.01 s^{-1}; (c): 350 °C and 1 s^{-1}; (d): 350 °C and 0.01 s^{-1}. The microstructures are characterized by compressed grains without the evidence of any recrystallisation.

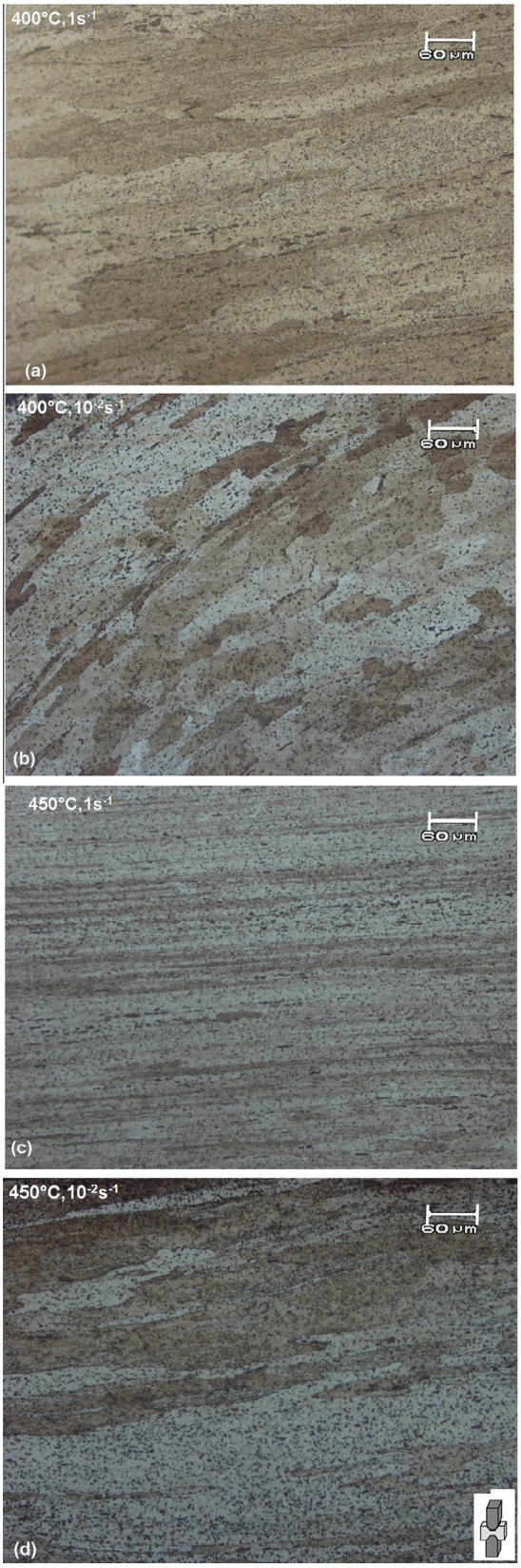

Fig. 6. Optical microstructures at the center of specimens deformed at (a): 400 °C and 1 s^{-1}; (b): 400 °C and 0.01 s^{-1}; (c): 450 °C and 1 s^{-1}; (d): 450 °C and 0.01 s^{-1}. The microstructures are characterized by the evidence of clear recrystallised grains.

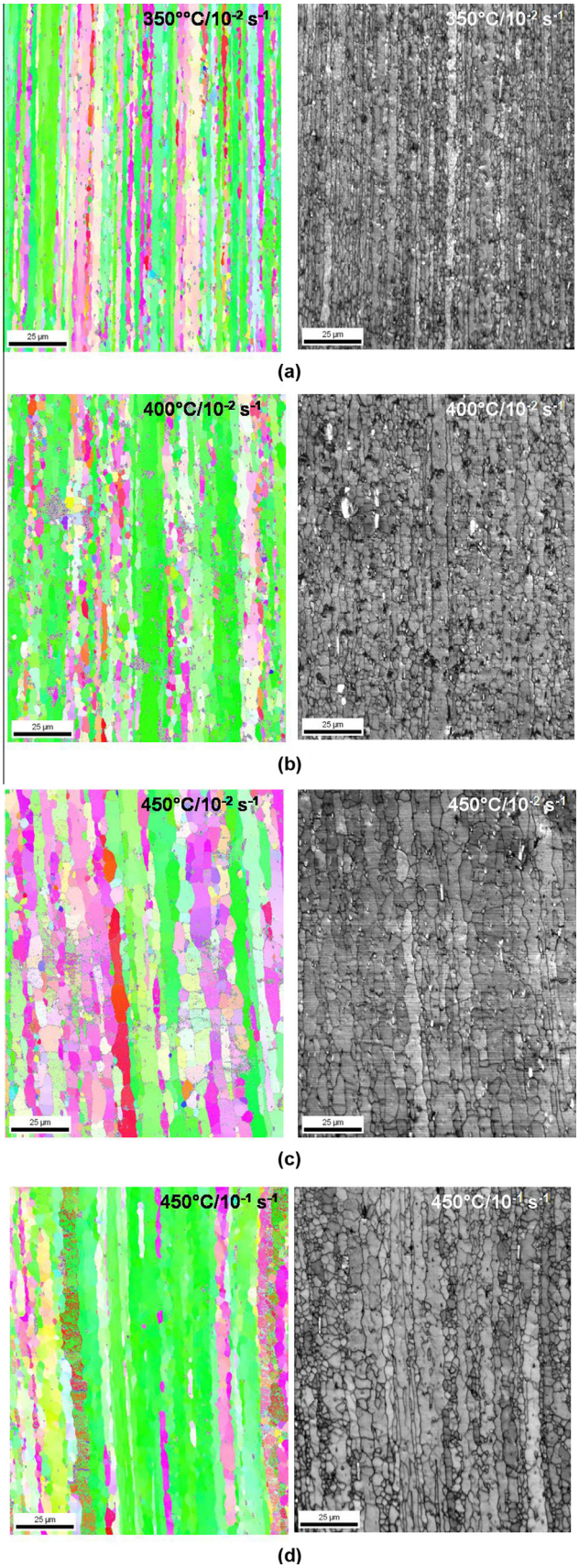

Fig. 7. Inverse pole figure and image quality map of Al–Li alloy sample deformed at (a) 350 °C at 10^{-2} s^{-1}, (b) 400 °C at 10^{-2} s^{-1}, (c) 450 °C at 10^{-2} s^{-1} and (d) 450 °C at 10^{-2} s^{-1}.

Table 2
Fraction of different type of grain boundaries in AA 2195 samples subjected to different modes of processing.

Sample	Very low angle grain boundary (VLAB, θ = 2–5°)	Low angle grain boundary (LAGB, θ = 5–15°)	High angle grain boundary (HAGB, θ > 15°)
350 °C 10^{-2} s^{-1}	8.4	12.2	79.4
400 °C 10^{-2} s^{-1}	5.0	5.1	89.8
450 °C 10^{-2} s^{-1}	6.1	3.9	90.0
450 °C 10^{-1} s^{-1}	9.1	9.1	81.8

distribution in all the four samples shown in Table 2 indicate the highest fraction of High Angle Grain Boundaries in the 450 °C sample deformed at 10^{-2} s^{-1} further substantiating dominant dynamic recrystallization. The evolution of intragranular misorientation parameters like Kernel Average Misorientation (KAM), which is the average misorientation of a pixel with its neighbouring pixels gives a direct estimate of intragranular dislocation activity., Grain Average Misorientation and Grain Orientation Spread also indicate formation of new strain free recrystallized grains. However, due to significant change in grain size in the deformed samples the GAM and GOS values do not show a particular trend. However, the KAM distribution sheds light on microstructural evolution in a lucid way.

The KAM distribution for all the samples is characterized by the presence of one peak at low angle less than 1° and another at high misorientation of 5° (Fig. 8a and b). It is observed that with increase in temperature, there is a decrease in low angle misorientation with increase in high angle misorientation. The low angle misorientation corresponds to the formation of dislocation substructure and the decrease in fraction of lower KAM value indicates decrease in dislocation density with increase in temperature. On the other hand, the 450 °C sample tested at higher strain rate shows an increase in the fraction of low KAM indicating increase in dislocation density of this sample. The aforementioned observations clearly indicate that the extent of DRX is highest at high temperature and low strain rate. This is further corroborated by decrease in volume fraction of ⟨101⟩ fibre component for the sample tested at 450 °C 10^{-2} s^{-1}. The orientation of newly formed recrystallized grains is different from the ⟨101⟩ fibre orientation which is the stable end orientation for plane strain compression of Al–Li alloy that deforms essentially by planar slip. A closer look at the misorientation distribution in terms of the cumulative misorientation distribution plot in Fig. 9 shows a higher fraction of low angle boundaries at lower temperature. Thus the process of conversion of low angle grain boundaries to high angle grain boundaries by the process of DRX is accelerated at high temperature. The sample deformed at high temperature and high strain rate shows relatively lower fraction of HAGB compared to slow strain rate deformed sample at the same temperature. This indicates that the process of conversion of LAGB to HAGB is not complete due to less time for dislocation rearrangement and interaction. However, lower grain size obtained at higher strain rate proves that the higher fraction of HAGB in the low strain rate sample is due to grain growth. The occurrence of grain growth is confirmed by higher grain size from the horizontal intercept compared to the vertical intercept for the 400 °C sample tested at slow strain rate. Thus an optimum combination of high temperature and high strain rate can be combined to obtain sub-micron grains in Al–Li alloy. The combined effect of temperature and strain rate is expressed in terms of the Zener–Hollomon parameter and it is observed that the grain refinement is higher that is the grain size is lower for higher Zener–Hollomon parameter.

It is to be mentioned here that aluminium–lithium alloys have historically suffered due to poor formability. One of the reasons for

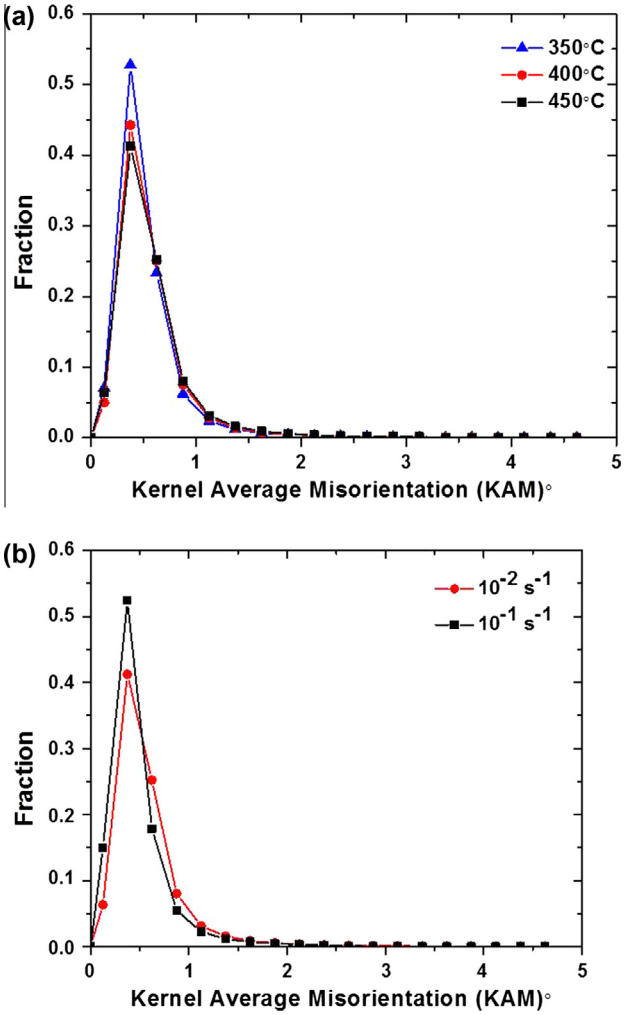

Fig. 8. Variation of KAM for the samples deformed at (a) different temperatures at a given strain rate of 10^{-2} s^{-1} and (b) at different strain rates at a given temperature of 450 °C.

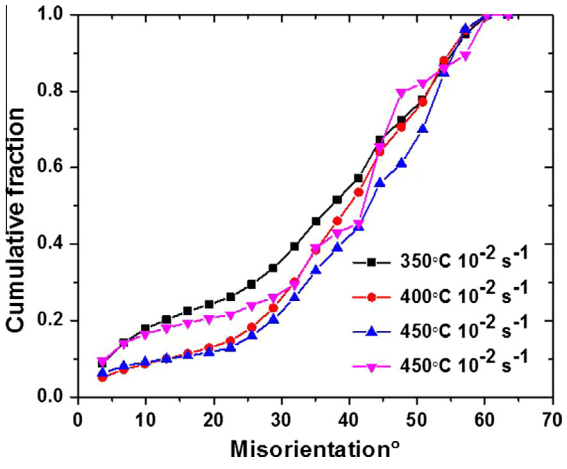

Fig. 9. Cumulative misorientation distribution in samples plane strain compressed tested under different conditions.

the poor formability is the presence of a strong Bs {101}⟨121⟩ component due to planar slip [24]. In order to monitor the evolution of crystallographic texture as a function of different processing conditions, volume fraction of important rolling texture components namely Cu{112}⟨111⟩, Bs {110}⟨112⟩, S {123}⟨364⟩, Cube {100}⟨001⟩ and Goss {110}⟨001⟩ was calculated from the EBSD scans. The volume fraction as depicted in Table 3 clearly show the presence of strong Bs and S component along with a weak Cu component in all the samples. However, the presence of weak ⟨101⟩ texture that is manifested in terms of lower Bs component accompanied with significant Cube component for the sample deformed at 450 °C at strain rate of 0.01. Thus choice of a proper thermomechanical processing condition providing more equiaxed and finer grain size with relatively weaker Bs texture may offer better formability.

Table 3
Volume fraction of the important rolling/plane strain deformation components in AA 2195 alloy processed by different routes.

Sample	Cube	Goss	Cu	Bs	S
350 °C 10^{-2} s^{-1}	0.8	0.4	2.2	26	27.9
400 °C 10^{-2} s^{-1}	0.4	1.8	1.4	24.1	11.8
450 °C 10^{-2} s^{-1}	3.1	0.4	4.3	13.6	22.6
450 °C 10^{-1} s^{-1}	2.7	0.5	1.1	37.8	14.2

4. Conclusions

Microstructural evolution during large strain deformation of aluminium–copper–lithium alloy AA 2195 has been studied using a single hit, hot isothermal plane strain compression (PSC) testing method in the temperature range of 300–450 °C and at strain rates of 0.01 s^{-1} and 1 s^{-1}.

(1) The flow curves during PSC exhibited weak softening at higher temperatures and dipping of the flow curve at a strain rate of 1 s^{-1}.
(2) Optical microstructure revealed compressed type grains in the specimens deformed at 300 °C and 350 °C, whereas clear stress free grain with wavy grain boundaries were noticed in specimens deformed at 400 °C and 450 °C.
(3) Electron backscattered diffraction analysis (EBSD) of the PSC tested samples confirmed that dynamic recrystallisation occurs in specimens deformed at higher temperatures and lower strain rates.
(4) Finally, it is possible to control the grain size in AA 2195 through the optimization of temperature and strain rate during thermo-mechanical processing.

Acknowledgement

The authors wish to thank Director, VSSC for granting permission to publish this work.

References

[1] Dursun T, Soutis C. Recent developments in advanced aircraft aluminium alloys. Mater Des 2014;56:862–71.
[2] Rioja RJ, Liu J. The evolution of Al–Li base products for aerospace and space applications. Metall Mater Trans A 2012;43:3325–37.
[3] Zhang SF, Zeng WD, Yang WH, Shi CL, Wang HJ. Ageing response of a Al–Cu–Li 2198 alloy. Mater Des 2014.
[4] Lynch S, Muddle B, Pasang T. Ductile-to-brittle fracture transitions in 8090 Al–Li alloys. Acta Mater 2001;49:2863–74.
[5] Rao KV, Yu W, Ritchie R. Cryogenic toughness of commercial aluminum–lithium alloys: role of delamination toughening. Metall Trans A 1989;20:485–97.
[6] Suresh S, Vasudevan A, Tosten M, Howell P. Microscopic and macroscopic aspects of fracture in lithium-containing aluminum alloys. Acta Metall 1987;35:25–46.
[7] Huang X, Richards N, Chaturvedi M. Effect of grain size on the weldability of cast alloy 718. Mater Manuf Processes 2004;19:285–311.

[8] Lathabai S, Lloyd P. The effect of scandium on the microstructure, mechanical properties and weldability of a cast Al–Mg alloy. Acta Mater 2002;50:4275–92.
[9] Murty S, Torizuka S, Nagai K, Kitai T, Kogo Y. Dynamic recrystallization of ferrite during warm deformation of ultrafine grained ultra-low carbon steel. Scripta Mater 2005;53:763–8.
[10] Narayana Murty S, Torizuka S, Nagai K. Microstructural and micro-textural evolution during single pass high Z-large strain deformation of a 0. 15 C steel. ISIJ international. 2005;45:1651–7.
[11] Narayana Murty S, Torizuka S, Nagai K, Koseki N, Kogo Y. Classification of microstructural evolution during large strain high Z deformation of a 0.15 carbon steel. Scripta Mater 2005;52:713–8.
[12] Nayan N, Murty S, Jha AK, Pant B, Sharma S, George KM, et al. Processing and characterization of Al–Cu–Li alloy AA 2195 undergoing scale up production through the vacuum induction melting technique. Mater Sci Eng A 2013;576:21–8.
[13] Nayan N, Murty S, Sharma S, Sreekumar K, Sinha P. Processing and characterization of Al–Cu–Li alloy AA2195. Mater Sci Forum: Trans Tech Publ 2012:119–24.
[14] Nayan N, Nair KS, Mittal M, Sudhakaran K. Studies on Al–Cu–Li–Mg–Ag–Zr alloy processed through vacuum induction melting (VIM) technique. Mater Sci Eng, A 2007;454:500–7.
[15] Puchi E, Staia M. Mechanical behavior of aluminum deformed under hot-working conditions. Metall Mater Trans A 1995;26:2895–910.
[16] Puchi E, Staia M. High-temperature deformation of commercial-purity aluminum. Metall Mater Trans A 1998;29:2345–59.
[17] Schotten K, Bleck W, Dahl W. Modelling of flow curves for hot deformation. Steel Res 1998;69:193–7.
[18] Cheng L, Xue X, Tang B, Liu D, Li J, Kou H, et al. Deformation behavior of hot-rolled IN718 superalloy under plane strain compression at elevated temperature. Mater Sci Eng A 2014;606:24–30.
[19] Zhang X, Liu Q, Wu X, Zhu A. Work softening and annealing hardening of deformed nanocrystalline nickel. Appl Phys Lett 2008;93:261907.
[20] Asaro RJ, Needleman A. Overview No. 42 texture development and strain hardening in rate dependent polycrystals. Acta Metall 1985;33:923–53.
[21] Sun P, Cerreta E, Gray III G, Bingert J. The effect of grain size, strain rate, and temperature on the mechanical behavior of commercial purity aluminum. Metall Mater Trans A 2006;37:2983–94.
[22] Semiatin S, Jonas J. Formability and workability of metals: plastic instability and flow localization. Ohio, USA: American Society for Metals; 1984.
[23] Srinivasan M, Goforth R. Studies on activation energy of superplastic dynamically recrystallized aluminum–lithium alloys. Scr Metall Mater 1994;31:1151–6.
[24] Jata KV, Panchanadeeswaran S, Vasudevan AK. Evolution of texture, micro structure and mechanical property anisotropy in an Al–Li–Cu alloy. Mater Sci Eng A 1998;257(1):37–46.